Orthorhombic full-waveform inversion and model building for azimuthal anisotropy in the presence of gas bodies

Shivaji Maitra, Fariza F. Basir, and M. Luqman Ghazali, CGG; Ahmad Riza Ghazali, and Sarmiza M. Sapiai, PETRONAS CARIGALI; Nabil El Kady, and Tugrul Konuk, Formerly PETRONAS CARIGALI*

Summary

Deriving high-resolution velocity models in heavily faulted areas is challenging. This can be further complicated by the presence of gas bodies at multiple depth levels. The use of full-waveform inversion (FWI), given long enough offset and a good starting model, is becoming common practice for resolving near surface gas bodies and high wavenumber velocity variations. Also, FWI can honor azimuthal velocity variations by propagating the wavefield through an orthorhombic medium when calculating the objective function.

In the presence of a principal stress orientation, a WAZ or FAZ dataset highlights the velocity variation with azimuth. If the velocity dependence on azimuth and velocity variations across faults are not properly addressed during wave propagation, they can pose severe challenges to imaging complex fault systems including mis-positioned faults and poor fault shadow imaging. To address these challenges, an orthorhombic full-waveform inversion (Ort-FWI) approach has been used to recover a high-resolution velocity model, addressing lateral velocity variations across faults or due to gas bodies, while honoring the azimuthal velocity variations. We show how Ort-FWI produces a high-resolution velocity model that improves fault focusing and heals fault and gas shadow effects. The combination of these improvements gives a clear uplift in the final seismic image.

Introduction

The field under study, located offshore Sarawak, Malaysia, is a highly faulted anticline with three-way dip closure and relatively flat flanks. It is severely affected by a regional compressional stress field which has re-activated an existing extensional basin (Tingay et. al., 2009). In all WAZ, MAZ or FAZ seismic data sets acquired in this, and adjacent areas, the stress field is manifested as azimuthal anisotropy.

In 1991, a conventional short-offset (3 km) streamer survey was shot over this field which lies in approximately 70 m of water depth. The streamer data had many limitations that led to structural uncertainties, unconstrained velocity variations, poor fault imaging and unsuccessful fault shadow imaging.

To address these challenges, PETRONAS acquired a high-density 3D 4C WAZ ocean bottom node (OBN) survey in 2016. The acquisition consisted of 42 rolling patches and one static patch to cover the area underneath fixed surface installations near the center of the survey (Figure 1a). The work effort put into this high-density OBN survey can be gauged by the fact that 3.8 billion traces were recorded in a survey area of 100 km^2. In-production 3D distributed acoustic sensing vertical seismic profiling (DAS-VSP) data was recorded simultaneously, for three wells, with the OBN static patch to help reduce uncertainty at the reservoir levels. The availability of rich azimuth (Figure 1b) and long offsets (12 km) leads to many advantages like better illumination, and better signal-to-noise (S/N) ratio. These can be further exploited in future amplitude versus azimuth studies if the event positioning and azimuthal image alignment is handled properly in anisotropic velocity model building and imaging.

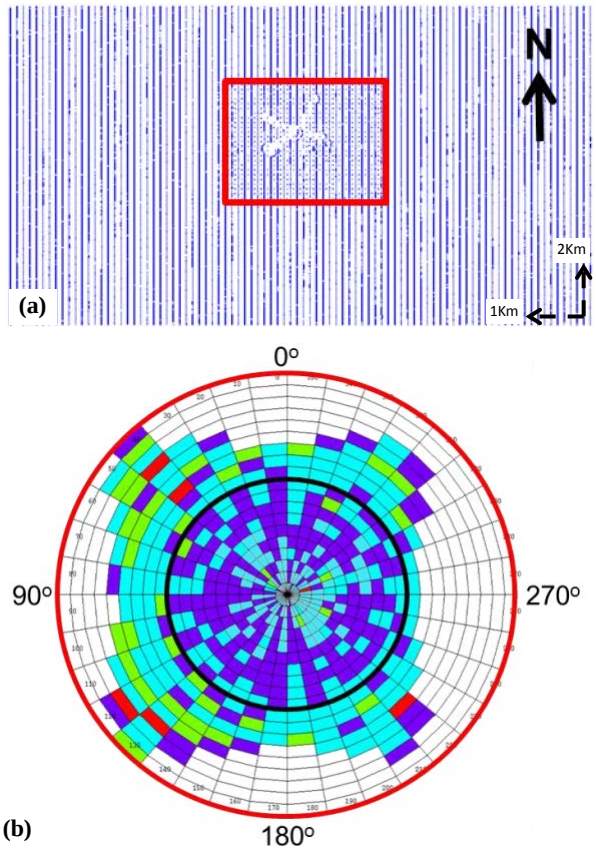

Figure 1: (a) Receiver Line map showing rolling and static patch (red box). (b) Rose map of survey. The red circle represents 12 km offset while the black circle represents 6 km (nominal) offset. The color code represents fold inside one common-offset-common-azimuth (COCA) sector.

10.1190/segam2018-2995810.1

Orthorhombic FWI and Model Building for Azimuthal Anisotropy in Presence of Gas Bodies

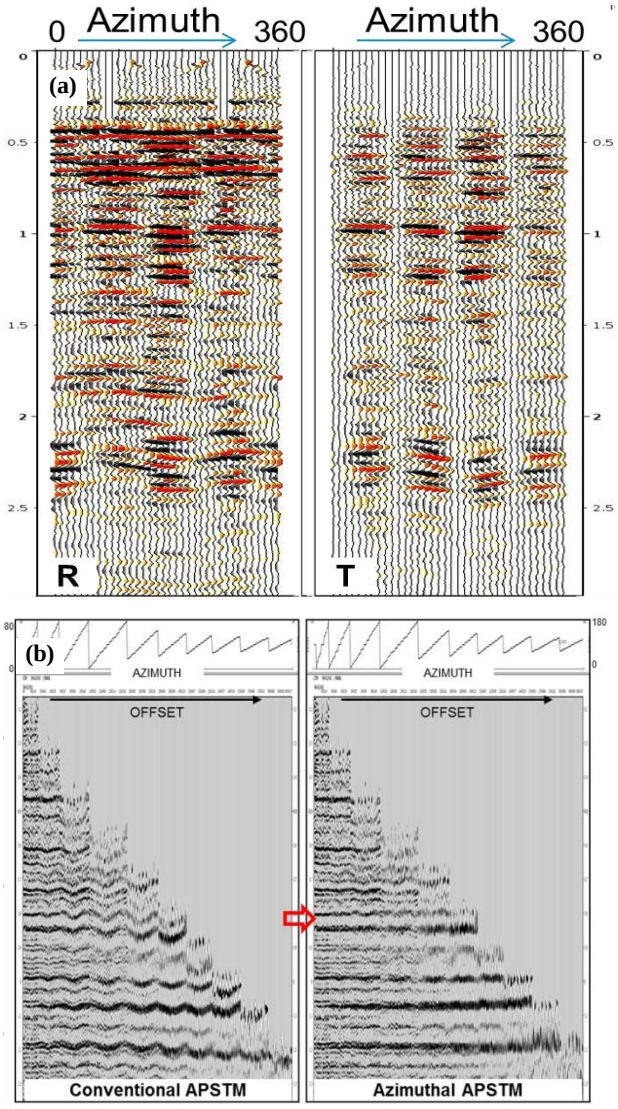

Figure 2: Indications for azimuthal anisotropy: (a) PS radial (R) and transverse (T) azimuthally sectored traces showing arrival time differences on the R and polarity reversals on T component. (b) PP-APSTM COCA gathers migrated using conventional APSTM and azimuthal APSTM. Azimuthal APSTM is able to resolve the jitter effect, to some extent, attributed to arrival time differences between the fast and slow P-waves.

Observing azimuthal anisotropy

Having access to a high-density four component WAZ data set was crucial to identifying azimuthal anisotropy in this field. The PS data set clearly showed shear-wave-splitting effects (Figure 2a) and this was further supported by azimuthal moveout effects seen on anelliptic prestack time migration (APSTM) common-offset-common-azimuth (COCA) gathers (Figure 2b). Stacking of such gathers will result in a degraded stack and can lead to poor post-migration seismic inversion studies.

Orthorhombic velocity estimation

Orthorhombic velocity modelling and orthorhombic anisotropy prestack depth migration (Ort-APSDM) are necessary to correctly solve the azimuthal variation in the wave propagation velocity (Xie et. al., 2016). Tsvankin (1997) described azimuthal anisotropy through 9 parameters: V_p, ε_1, δ_1, ε_2, δ_2, δ_3, ϕ, θ and α, where V_p is the vertical velocity of the P-wave, ε_1 and δ_1 describe the anisotropy parameters in the fast direction, ε_2 and δ_2 describe the anisotropy in the slow direction, δ_3 describes the anisotropy along the reflectors, ϕ describes the azimuth of dipping reflector, θ describes the dip of reflectors, and α describes the azimuth of slow direction. Following Tsvankin (1997) and Alkhalifah (2003), Xie et al. (2011) proposed to represent the phase velocity for the orthorhombic media in the following form, which removes the weak anisotropy restriction (here $V(\theta,\alpha)$ is the phase velocity):

$$\frac{V^2(\theta,\alpha)}{V_{p_0}^2} = \frac{\left(1 + 2\,\varepsilon(\alpha)\sin^2\theta + \sqrt{(1 + 2\,\varepsilon(\alpha)\sin^2\theta)^2 - 8\big(\varepsilon(\alpha) - \delta(\alpha)\big)\sin^2\theta\cos^2\theta}\right)}{2}$$

where,

$$\varepsilon(\alpha) = \varepsilon_1 \sin^4\alpha + \varepsilon_2 \cos^4\alpha + (2\varepsilon_2 + \delta_3)\sin^2\alpha\cos^2\alpha$$
$$\delta(\alpha) = \delta_1 \sin^2\alpha + \delta_2 \cos^2\alpha$$

To create an initial orthorhombic model, the WAZ data was split into four azimuth sectors and the velocity for each individual azimuth sector was updated independently using tomography. This approach minimized the residual curvature on common image gathers (CIGs).

An initial orthorhombic model was then generated using the equations above. Using this model for Ort-APSDM helped to resolve azimuthal move-out differences in the COCA gathers as shown in Figure 3.

The orthorhombic model could be updated further through tomographic updates. However, for a stable tomographic inversion, regularization and smoothing are required. This limits the resolution of tomographic inverted velocity models. To fully resolve velocity contrasts across gas bodies and mitigate fault shadow issues, tomography requires additional geologic constraints like faults and horizons. This can be impractical in cases like this field where there are multi-level gas bodies and complex fault systems of numerous major and minor faults.

To handle this challenge Ort-FWI was run using the initial orthorhombic model as the starting point. Ort-FWI uses the orthorhombic parameters during the wavefield propagation. This helps the synthetic (predicted) shots honor the real

10.1190/segam2018-2995810.1

world anisotropy and produce a more accurate velocity model update that conforms to the orthorhombic anisotropy (Xie et al., 2016).

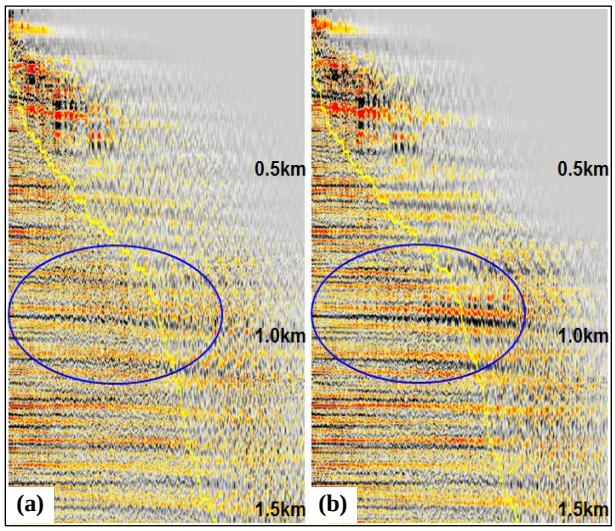

Figure 3: (a) Azimuthal moveout seen as jitters on COCA gathers after vertically transverse isotropy (VTI) APSDM, and (b) Ort-APSDM showing that the jitter effect is resolved by using an orthorhombic model.

Assuming that the objective function only reflects the required change in velocity, Ort-FWI was run to update V_p only, by minimizing the mismatch between the real data and forward modelled synthetic shots through the orthorhombic model. The minimization of this function was done using the time domain, preconditioned, steepest-descent algorithm as described by Ratcliffe et al. (2014).

The overall strategy used for orthorhombic model update is as follows:

1. Tomographic update of 4 azimuth sectors to create initial orthorhombic model.
2. Ort-FWI to create a high-resolution V_p model so as to resolve gas bodies and fault shadow effects arising from high-wavenumber variations in the velocity field.
3. Update azimuthally anisotropic parameters ε_1, δ_1, ε_2, δ_2, through orthorhombic tomography and migration scan picking for α.
4. Tomographic update for V_p, ε_1, δ_1, ε_2, δ_2, and δ_3 for deeper reflectors not illuminated by diving waves.

For this survey, Ort-FWI was run from 2 to 8 Hz, using frequency marching and all recorded diving wave energy up to 12 km offset. A spatially high-resolution V_p model was thus obtained. Validity of the updated model was confirmed by running subsequent QCs such as: i) the cost function stabilized; ii) residual curvatures picked on migrated CIGs showed a significant improvement (from ±5% to ±2%); and iii) average cross-correlation between real and synthetic shots increased from 0.3 to 0.9.

Figures 4 and 5 show how Ort-FWI is able to delineate shallow gas bodies (red arrows), individual fault blocks (white arrows), gas charged faults (yellow arrow) and deep buried gas bodies (orange arrow) within the velocity model. Comparison of Figures 6 and 7 show the impact of Ort-FWI in imaging improvements between initial and updated orthorhombic FWI model, where geological structures are both simplified in their form (red arrow) and enhanced in their strength (yellow oval).

This Ort-FWI model was also useful to guide two iterations of Q-tomography which resulted in a high resolution Q model. This was used for the final Q-Ort-APSDM.

Discussions

In the absence of PS data it becomes imperative to look out for azimuthal variations of velocity as early as possible in the model building workflow. This would avoid unnecessary delays like in this study, where FWI had to be re-started using an initial orthorhombic model to get meaningful updates, especially underneath shallow gas bodies.

Further work on this survey involves running Reverse Time Migration (Q-Ort-RTM) using the final models, as well as integrating the three DAS-VSP data sets which should help to reduce uncertainty at reservoir level even further.

The final migrated gathers show good image alignment over all azimuths and are good candidates for amplitude versus azimuth studies which should give further insights into the nature of this reservoir.

Conclusion

The model update strategy defined here and used in this project allows all data from WAZ OBC surveys to be used in orthorhombic FWI without worrying about variations in velocity between different azimuths.

The positive impact of Ort-FWI is clearly observed in the improved Ort-APSDM image. The result shows significant ability to resolve fault and gas shadow effects on the deeper reflectors, which are the oil producing reservoirs. This enables better interpretation of geologically plausible structures and helps de-risk future production wells.

Acknowledgements

The data used in this study belongs to PETRONAS Carigali Sdn Bhd. The authors appreciate PETRONAS and CGG management for permission to present these result.

10.1190/segam2018-2995810.1

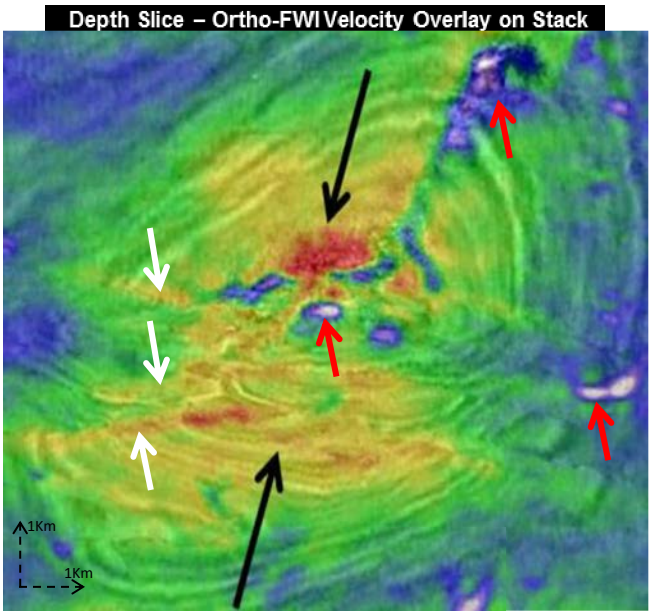

Figure 4: Black arrows show the direction of regional stress on a shallow depth slice of the Ort-FWI velocity field overlaid on stack. Red arrows show shallow gas bodies, while white arrows show fault planes delineated by FWI.

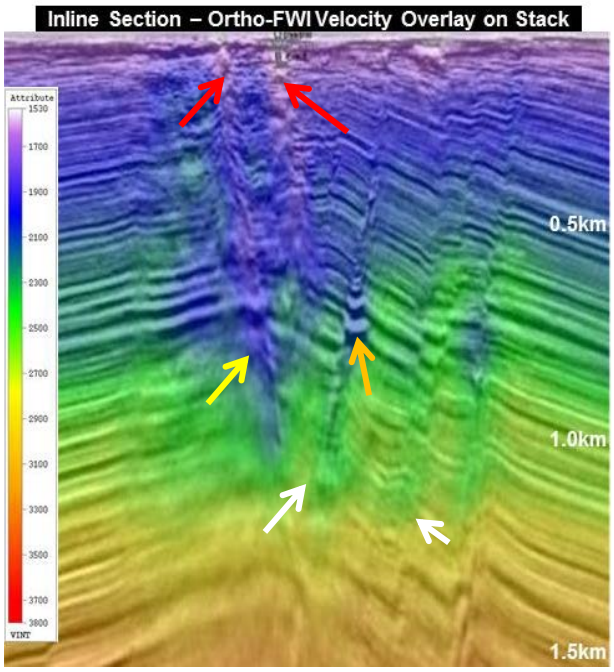

Figure 5: Inline section of Ort-FWI velocity overlaid on a migrated stack showing delineation of individual fault blocks, shallow gas, gas charged faults and deep buried gas bodies. Red and white arrows show gas bodies and fault planes respectively.

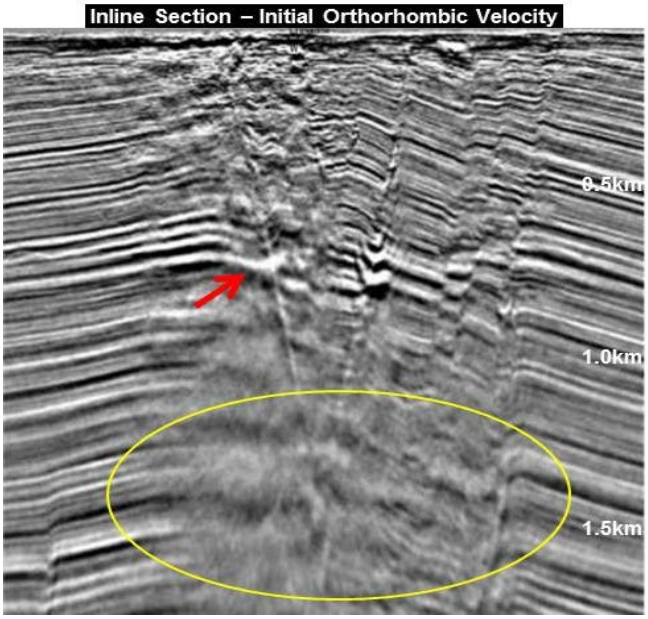

Figure 6: APSDM stack migrated using the initial orthorhombic model.

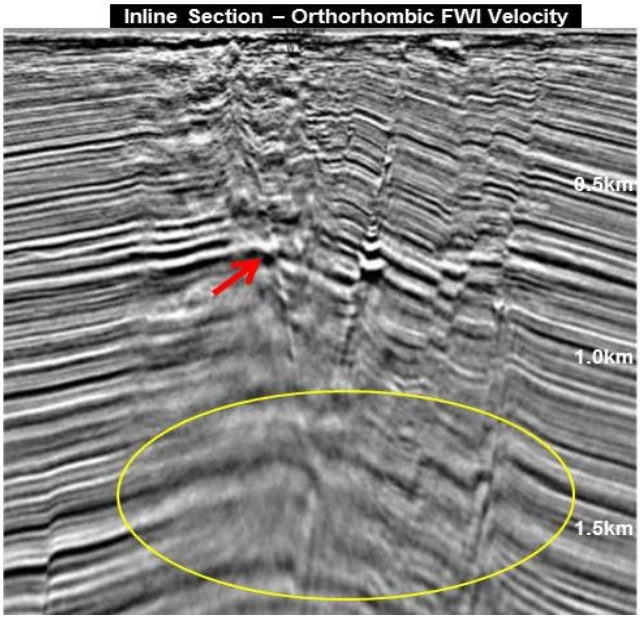

Figure 7: APSDM stack migrated with the Ort-FWI model, showing significant improvement in resolving fault shadow effect, marked by the red arrow, and improved imaging of deeper reflectors, marked by the yellow oval.

10.1190/segam2018-2995810.1

REFERENCES

Alkhalifah, T., 2003, An acoustic wave equation for orthorhombic anisotropy: Geophysics, **68**, 1169–1172, https://doi.org/10.1190/1.1598109.

Ratcliffe, A., A. Privitera, G. Conroy, V. Vinje, A. Bertrand, and B. Lyngnes, 2014, Enhanced imaging with high- resolution fullwaveform inversion and reverse time migration: A North Sea OBC case study: The Leading Edge, **33**, 986–992, https://doi.org/10.1190/tle33090986.1.

Tingay, M., C. Morley, R. King, R. Hillis, and D. Coblentz, 2009, Southeast Asian stress map: Implications for petroleum exploration and production: First Break, **27**, 81–88.

Tsvankin, I., 1997, Anisotropic parameters and P-wave velocity for orthorhombic media: Geophysics, **62**, 1292–1309, https://doi.org/10.1190/1.1444231.

Xie, Y., S. Birdus, J. Sun, and C. Notfors, 2011, Multi-azimuth seismic data imaging in the presence of orthorhombic anisotropy: 73rd Annual International Conference and Exhibition, EAGE, Extended Abstracts, G022, https://doi.org/10.2523/IPTC-16682-MS.

Xie, Y., B. Zhou, J. Zhou, J. Hu, L. Xu, X. Wu, N. Lin, and Z. Wang, 2016, Orthorhombic full-waveform inversion for wide-azimuth data imaging: 86th Annual International Meeting, SEG, Expanded Abstracts, 1289–1293, https://doi.org/10.1190/segam2016-13822505.1.

Warner, M., A. Ratcliffe, T. Nangoo, J. Morgan, A. Umpleby, N. Shah, V. Vinje, I. Stekl, L. Guasch, C. Win, G. Conroy, and A. Bertrand, 2013, Anisotropic 3D full-waveform inversion: Geophysics, **78**, no. 2, R59–R80, https://doi.org/10.1190/geo2012-0338.1.